Applied Energy 243 (2019) 175–190

Contents lists available at ScienceDirect

Applied Energy

journal homepage: www.elsevier.com/locate/apenergy

Optimization of thermal performance in thermocline tank thermal energy storage system with the multilayered PCM(s) for CSP tower plants☆

K.E. Elfeky[a], Xinyi Li[a], N. Ahmed[a], Lin Lu[b], Qiuwang Wang[a,*]

[a] Key Laboratory of Thermo-Fluid Science and Engineering, Ministry of Education, School of Energy and Power Engineering, Xi'an Jiaotong University, Xi'an, Shaanxi 710049, PR China

[b] Department of Building Services Engineering, The Hong Kong Polytechnic University, Hung Hom, Kowloon, Hong Kong, China

HIGHLIGHTS

- Thermal performance of multilayered PCM(s) thermocline TES tank is analyzed.
- A numerical model is used for the thermal evaluation of thermocline configurations.
- A parametric study of PCM melting temperature and heat of fusion is performed.
- Results indicated the optimal values of melting temperature and latent heat for MLSPCM(s).

ARTICLE INFO

Keywords:
Thermal energy storage
Concentrating solar power plants
Encapsulated phase change material
Multilayered phase change materials
Thermocline tank

ABSTRACT

The current paper presents two parametric studies (inverse Stefan number and dimensionless temperature difference) to optimize the values of latent heat and melting temperature of multilayered phase change materials (MLPCM(s)) in thermocline tank for concentrating solar power (CSP) plants. Spherical capsules filled with PCM (s) of different thermo-physical properties are used to fill the bed region, and the molten salt is used as heat transfer fluid (HTF). The numerical model that has been developed uses the Dispersion-Concentric (D-C) equations. By using MATLAB, the governing equations are solved and validated against the experimental results. The results show that in the optimal configuration of the case (B), the values of *InvSte* number and dimensionless temperature (θ_m) are equal to 1.2 and 0.8 for the top PCM layer, respectively; 0.75 and 0.55 for the middle PCM layer, respectively; and 0.65 and 0.3 for the bottom PCM layer, respectively. Moreover, it is also found that to obtain the best design and distribution of temperature for a thermocline tank consisting of three layers of PCM, the top PCM layer should melts by $\Delta T = 55.4$ °C below the HTF charging inlet temperature, the PCM layer at the bottom should solidifies by $\Delta T = 83.1$ °C above HTF discharging inlet temperature.

1. Introduction

Thermal energy storage (TES) is a key element in interrupted energy conversion cycles like concentrating solar power (CSP) plants, where there is a mismatch between the solar energy supply and electricity demand [1,2]. While, sensible heat storage presently controls the market for such kind of TES technology [3–5]. In recent years, latent heat thermal energy storage (LHTES) systems have demonstrated the ability to use as a real alternative to traditional TES systems [6,7]. These systems use single and multilayered phase change materials (MLPCM(s)) configurations [8,9]. PCM(s) provide more compact designs than sensible heat storage, which can lead to lower storage media costs [10,11]. However, LHTES of the salt hydrates PCM(s) suffers from low thermal conductivity. This leads to decrease the rate of heat transfer during charge and discharge cycle. There are different ways that have been investigated to overcome this issue. Macro-encapsulation of the PCM inside a hollow shell is one of the methods that have been used to increase the rate of the heat transfer, therefore the thermal performance of the system become more efficient [7]. Several experimental and numerical studies have been carried out to improve heat transfer performance of the encapsulated PCM during phase change process [12–14]. For the charge cycle, the process of heat

☆ Presented at the 10th International Conference on Applied Energy (ICAE2018), 2018.8.22–8.25, Hong Kong, China. (Original paper title: "Numerical investigation of the melting temperature effect on the performance of thermocline thermal energy storage tank for CSP" and Paper number 597).

* Corresponding author.
E-mail address: wangqw@mail.xjtu.edu.cn (Q. Wang).

https://doi.org/10.1016/j.apenergy.2019.03.182
Received 2 January 2019; Received in revised form 27 February 2019; Accepted 21 March 2019

Nomenclature

A_{bed}	area of bed cross section, m^2
c_p	specific heat capacity, $J{\cdot}kg^{-1}{\cdot}K^{-1}$
D_{bed}	diameter of storage tank, m
d_p	diameter of PCM spheres, m
d_r	reference diameter, m
d_j	diameter of insulation layer j, m
E_{stored}	energy stored in PCM particles, J
E_{pump}	pumping energy, J
E_{input}	input energy, J
$E_{outflow}$	energy extracted from tank, J
Emax stored	maximum theoretical energy can be stored, J
g	gravity, $m{\cdot}s^{-2}$
H	storage tank height, m
h	heat transfer coefficient, $W{\cdot}m^{-2}{\cdot}K^{-1}$
h_f	volumetric heat transfer coefficient between fluid and solid, $W{\cdot}m^{-2}{\cdot}K^{-1}$
h_{fs}	heat of fusion, $J{\cdot}kg^{-1}$
h_w	volumetric heat transfer coefficient between tank and ambience, $W{\cdot}m^{-2}{\cdot}K^{-1}$
k	thermal conductivity, $W{\cdot}m^{-1}{\cdot}K^{-1}$
$\dot{m}$	mass flow rate, $kg{\cdot}s^{-1}$
m	mass, kg
Nu	Nusselt number
N_x	nodes in axial direction
n	number of insulations
Pr	Prandtl number
ΔP	pressure drop, Pa
Ra	Rayleigh number
Re	Reynolds number
R_x	nodes within each sphere
r	radius of PCM spheres, m
T	temperature, K
T_m	melting temperature, K
T_{p2}	peak temperature of PCM during solid–liquid transition, K
T_{p1}	peak temperature of PCM during solid–solid transition, K
T_{ini}	initial bed temperature, K
T_{inf}	ambient temperature, K
ΔT	temperature difference, K
t	time, s
u_f	fluid velocity, $m{\cdot}s^{-1}$
X	non-dimensional height of tank
x	axial direction

Greek symbols

ε	average bed porosity
μ	dynamic viscosity, $kg{\cdot}m^{-1}{\cdot}s^{-1}$
ν	kinematic viscosity, $m^2{\cdot}s^{-1}$
η	energy efficiency
γ	utilization ratio
ρ	density, $kg{\cdot}m^{-2}$
θ	dimensionless temperature difference
σ	capacity ratio

Subscripts

ave	average
ch	charging
disch	discharging
c	cold
f	fluid
in	inlet
InvSte	inverse Stefan number
j	index for insulations
l	liquid PCM
m	melting point
out	outlet
p	particle of the PCM
sup	supplied
s	solid

Superscripts

i	index for time step
max	maximum

Abbreviations

CSP	concentrating solar power
HTF	heat transfer fluid
LF	liquid fraction
LHTES	latent heat thermal energy storage
MLPCM(s)	multilayered phase change materials
TES	thermal energy storage

transfer is directly proportional to the temperature difference between HTF and the PCM melting temperature; the rate of heat transfer is expected to be less at the lower section of the thermocline tank. Thus, the high rate of heat transfer can be kept by using different stages of PCM(s) particles while reducing melting temperature of the PCM layers along the thermocline tank. The HTF during charging cycle flows from the upper to the lower section, after the energy is been stored in the PCMs layers. Because of the continuous variation of PCM(s) properties (heat of fusion and melting temperature) with the HTF temperature over the height of the thermocline tank for single layer configuration, so, this is not a workable or economic way. The TES system is consists of a set of layers; all layers are filled with PCM(s) particles of different thermo-physical properties. This design will establish a more consistent between the HTF charge temperature and the PCM(s) layer melting temperature. That's the goal of using a MLPCM(s) thermocline tank TES system. In order to increase the efficiency of the CSP plants to produce electricity, advanced systems for high temperatures are presently being developed by heating the HTF to about 565 °C [15–17].

MLPCM(s) thermocline tank TES system configurations are investigated by a number of researcher's [18,19]. The main idea of this configuration is the containment of high and low melting temperature of PCM(s) particles as filler materials at the end sections of the thermocline tank, close to the inlet and outlet ports. In our previous study, Elfeky et al. [8] investigated the thermal performance of one layer PCM at different thermo-physical properties and MLPCM(s) configuration. The study exhibited that the MLPCM(s) configuration provided the best overall and exergy efficiency for the charge/discharge cycles. Furthermore, the study showed that the MLPCM(s) configuration could increase the rate of heat transfer and decrease charge/discharge time of the cycle. Zhao et al. [20] investigated the influence of the fill ratio of the encapsulated PCM(s) particles on the dynamic performance of the MLPCM(s) thermocline tank TES system. Zanganeh et al. [21] studied MLPCM(s) thermal storage systems by using air as HTF to fill the pore volume in the thermocline tank. In this design a thin layer of PCM particles of high melting point was placed at the top section of the thermocline tank. The results showed that the PCM layer contributed to make the outflow temperature more stable, but had no effect on the overall efficiency of charge/discharge cycles. Flueckiger et al. [22] applied and developed a new finite volume approach to study the thermal performance of LHTES thermocline tank with MLPCM(s) for

CSP plants, and a better approach to select the melting point of the PCM for this configuration at low computational cost. The results show that there is a severe improvement in the system performance, utilization ratio, and capacity factor when the melting temperature of the PCM(s) falls between the charging and discharging cut-off temperatures. Cheng et al. [23] studied the thermal performance of MLPCM(s) configuration, and compared with those of a single stage PCM. The studies demonstrated that, the MLPCM(s) has the best thermal performance, as it showed a 15.1% reduction in charging time compared to a single stage PCM. Wu et al. [24] investigated the thermal performance molten salt packed bed LHTES system, and their results showed that the discharging efficiency of the system can be improve by increasing the PCM melting temperature. Yang et al. [25] made a numerical study on a solar heat TES packaged bed for MLPCM(s) system. Recently, many researchers focused on the MLPCM(s) system, which aims to decrease charging/discharging time and improve charging/discharging efficiency of TES system [26,27]. Aldoss et al. [28] studied the thermal performance of MLPCM(s) thermocline tank, and the results of their studies showed that the MLPCM(s) configurations helped to enhance the rate of charge/discharge, increased heat transfer rate and improved storage capacity. Li et al. [29] investigated the dynamic responses of combined cycle gas turbine power plant integration with cascaded LHTES. In the last few decades, most of the works on energy storage in CSP mainly focused on molten salts technology [30,31]. Nithyanandam et al. [32] conducted an extensive parametric study in terms of non-dimensional parameters for molten salts thermocline tank TES with PCM as filler material to identify the optimum design and operating parameters for CSP plants. The results showed that the phase transition temperature must correspond to a value that is either above the discharging cut-off temperature or below the charging cut-off temperature to maximize usage of the potential storage capacity of thermocline tank.

Due to the complex dynamic nature of thermal performance of the latent heat storage system and the high cost of the experimental setups, it is necessary to look for numerical models to study the thermal performance of this system in different ways to understand the cycle of heat transfer between solid PCM(s) and the heat transfer fluid. Thermal performance of the thermocline tank system has been predicted numerically by using several different models. Ismail et al. [33] numerically investigated the dynamic performance of the thermocline storage tank with PCM(s) particles as filler material by using the (D-C) approach. The marching technique has been applied to check the numerical model within the particles of the PCM and then the process of phase transition was balanced with the energy equation on the surface of the PCM particles. Yang et al. [34] studied the dynamic performance of the thermocline tank TES during discharge cycle. The effects of a combination of different parameters (height of the tank, mass flow rate of HTF and diameter of the particle) on the dynamic performance of the tank were studied. The thermocline tank TES system performance was compared and presented by using various numerical models. Esence et al. [35] made a survey on the thermal performances and numerical studies of thermocline TES systems.

The single and MLPCM(s) configurations of different thermo-physical characteristics were carefully analyzed in our previous study Elfeky et al. [8], whereby the recommended design is the MLPCM(s) configuration. The thermal performance of LHTES systems can be strongly affected by different parameters; two of such parameters that have not been widely studied are the melting temperature and the heat of fusion [22]. The current study focuses on numerical investigation of the thermal performance of thermocline tank for charge/discharge cycles to optimize the values of latent heat and melting temperature of MLPCM(s) configurations. Hypothetical PCM(s) are used either in the top, middle or bottom section of the thermocline tank in order to investigate the effect of their thermal performance. The thermal performance study examines the heat transfer mechanisms in the thermocline tank that prevent the full use of storage capacity in MLPCM(s) design systems. Also, the issues encountered for the selection of PCM(s) are discussed. This paper considered two parametric studies (inverse Stefan number and dimensionless temperature difference) to optimize the values of latent heat and melting temperature of MLPCM(s) through which the overall efficiency of the thermocline tank TES system could be improved.

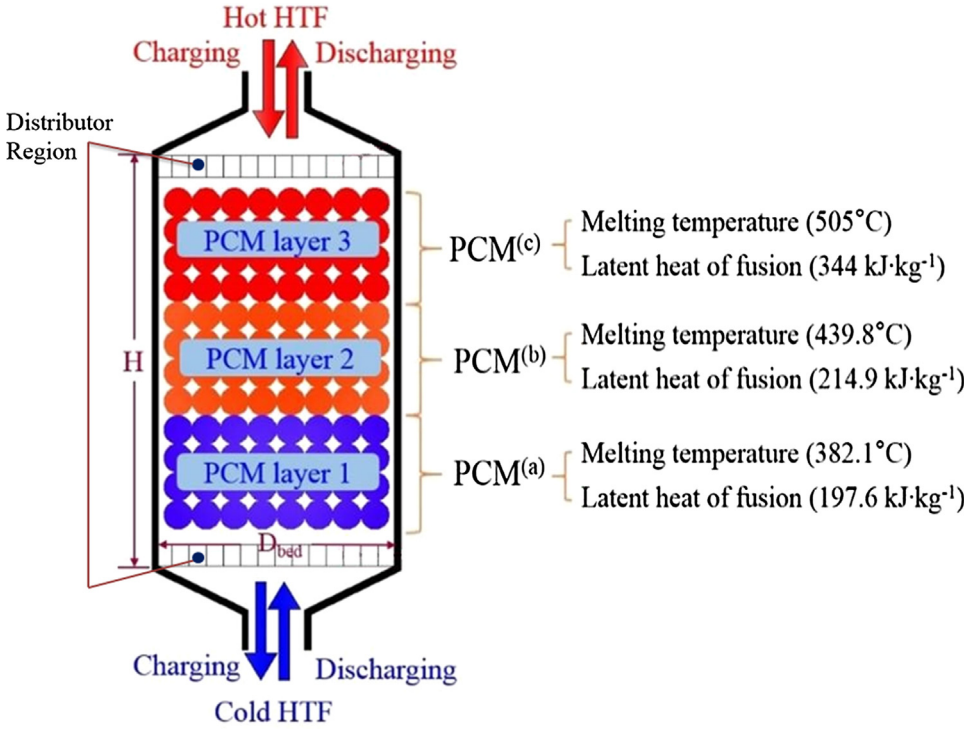

Fig. 1. Schematic diagram of MLPCM(s) thermocline tank TES configuration.

2. Numerical analysis

2.1. Model description and governing equations

MLPCM(s) thermocline tank systems provide efficient TES because of the efficiency of the high rate heat transfer. Fig. 1 schematically shows the structure of the MLPCM(s) configuration. The components of the storage tank are a vertical cylindrical tank and two main distributors; one of them at the inlets and the other at the outlet. During the storage charge cycle, hot HTF at temperature T_h, enters from the top of the tank, exchanges energy with the PCM(s) particles and comes out from the bottom of the tank. During the discharge cycle, cold HTF enters from the bottom of the tank at temperature T_c, recovers heat from the PCM(s) particles, and comes out from the top of the tank. The height and the diameter of the thermocline storage tank are denoted by H and D_{bed} respectively. The packing region is occupied by PCM(s) particles as filler material, which has porosity equal to 0.22.

The operating conditions considered in this study are summarized in Table 1. The thermo-physical properties of HTF can be found in Ref. [36]. These are defined below as:

$$\rho(\mathrm{kg\,m^{-3}}) = 2090 - 0.6357T(^{\circ}\mathrm{C}) \tag{1}$$

$$\mu(\mathrm{Ns\,m^{-2}}) = [22.714 - 0.12T(^{\circ}\mathrm{C}) + 2.281\times10^{-4}\cdot T^2(^{\circ}\mathrm{C}) - 1.474\times10^{-7}\cdot T^3(^{\circ}\mathrm{C})]\times10^{-3} \tag{2}$$

$$c_p(\mathrm{J\,kg^{-1}K^{-1}}) = 1443 - 0.172T(^{\circ}\mathrm{C}) \tag{3}$$

$$k(\mathrm{W\,m^{-1}K^{-1}}) = 0.443 + 1.9\times10^{-4}T(^{\circ}\mathrm{C}) \tag{4}$$

In this paper, the packing region consist of three equal parts as shown in Fig. 1, where by each part is completely charged with different PCM(s) particles; and are named as follows: PCM$^{(a)}$, PCM$^{(b)}$ and PCM$^{(c)}$.

The PCM(s) arrangements in this study have been done based on the melting temperature and heat of fusion, ordering from high to low (PCM$^{(c)}$ to PCM$^{(a)}$). Thermo-physical properties of the selected PCM(s) materials are suitable for the MLPCM(s) TES system. The PCM(s) are selected for MLPCM(s) based on two parametric studies and will be discuss in details in Section 2.5. The MLPCM(s) selection criteria can be found in our previous work [8].

The selection criterion of PCM(s) for the MLPCM(s) system design is based on several possible scenarios. The current work evaluates the effect of two parametric studies for a set of hypothetical PCM(s) of MLPCM(s) configurations system. The goal of this design is to determine a suitable combination of PCM(s) layers that will increase the energy output from the storage tank and compare the thermal performance of these different combinations with the basic case. The PCM(s) thermo-physical properties that have been used in the current study are shown in Table 2, as reported in [37].

In the present work, a transient Dispersion-Concentric (D-C) numerical model has been applied to describe how heat travels within the thermocline tank TES. This model considers the thermocline tank like a porous structure composed of separate particles of MLPCM(s) [38]. The following assumptions are made:

(1) The thermocline tank has three layers of insulation.
(2) The HTF flow from top to bottom during charge and vice versa during discharge.
(3) The distributors are not included in the numerical model and each PCM(s) particle is treated as a symmetric and divided into equal spaces.
(4) The heat lost by the tank wall from the upper and lower sides is very small and therefore neglected.
(5) The thermo-physical properties are determined based on the inlet/outlet temperature of the HTF, $T_{ave} = (T_{in} + T_{out})/2$ [39].
(6) The heat transfer by radiation inside the tank is neglected and no heat generation inside the tank.

The governing equations for the HTF and PCM(s) particles have been solved based on the above assumptions as follows:

For the fluid phase:

$$\varepsilon\rho_f c_{p,f}\frac{\partial T_f}{\partial t} + \varepsilon u_f\rho_f c_{p,f}\frac{\partial T_f}{\partial x} = \varepsilon k_f\frac{\partial^2 T_f}{\partial x^2} + h_f(T_s - T_f) + h_w(T_w - T_f) \tag{5}$$

For the solid phase:

$$(1-\varepsilon)\rho_s c_{p,s}\frac{\partial T_s}{\partial t} = (1-\varepsilon)k_s\frac{\partial^2 T_s}{\partial x^2} + h_f(T_f - T_s) \tag{6}$$

The temperature distribution on the surface of the PCM(s) particles can be calculated from:

$$\rho_s c_{p,s}\frac{\partial T_p}{\partial t} = \frac{1}{r^2}\frac{\partial}{\partial r}\left(k_s r^2\frac{\partial T_p}{\partial r}\right) \tag{7}$$

The volumetric heat transfer coefficient h_f for thermocline TES tank is determined from [40]:

$$h_f = \frac{6(1-\varepsilon)h_{overall}}{d_p} \tag{8}$$

where $h_{overall}$ is overall heat transfer coefficient for single PCM.

$$h_{overall} = \frac{1}{R_{ext} + R_{coat}} \tag{9}$$

where R_{ext} and R_{coat} are the external resistance on the surface of the PCM particle and resistance due to coating, respectively.

$$Re_p = \frac{\rho_f d_p \varepsilon u_f}{\mu_f},\ Pr = \frac{c_{p,f}\mu_f}{k_f} \tag{10}$$

The coefficient of heat loss from the wall of the tank h_w is calculated from [41].

$$h_w = \frac{h'(\pi D_{bed})}{\pi D_{bed}^2/4} = \frac{4h'}{D_{bed}} \tag{11}$$

$$\frac{1}{h'} = \frac{1}{h_{in}}\frac{d_r}{D_{bed}} + \frac{D_{bed}}{2}\sum_{j=1}^{n}\frac{1}{k_j}\ln\frac{d_{j+1}}{d_j} + \frac{1}{h_{out}}\frac{d_r}{d_{n+1}} \tag{12}$$

VDI Wärmeatlas [39] correlation has been used to solve natural

Table 1
Main characteristics of the MPCM(s) thermocline tank.

Parameters	Values
Height of tank (H)	7.376 m
Diameter of tank (D_{bed})	10.593 m
Diameter of PCM capsule (d_p)	0.02653 m
PCM shell thickness	0.00045 m
Tank wall thickness	0.0508 m
Rock wool insulation thickness	0.5 m
Flexible ceramic wool insulation thickness	0.02032 m
Tank wall thermal conductivity	20.0165 W/m-K
Rock wool thermal conductivity	0.06 W/m-K
Flexible ceramic wool thermal conductivity	0.12 W/m-K
PCM shell thermal conductivity (Alumina coating)	13.94 W/m-K
Mass flow rate ($\dot{m}$)	84.5175 kg/s
Heat transfer fluid (HTF)	60% $NaNO_3$ & 40% KNO_3
Phase change material (wt%)	1–59.98% $MgCl_2$-20.42% KCl-19.6% NaCl 2–55% $MgCl_2$-45%NaCl 3–35%Li_2CO_3-65 wt%K_2CO_3
Effective working temperature ranges (HTF)	288–565 °C
Charging cut-off temperature	396 °C
Discharging cut-off temperature	493 °C
Charge/Discharge time	400 min
Nodes in axial direction (Nx)	300
Nodes within each sphere (Rx)	30

Table 2
Thermo-physical properties of the MLPCM(s).

Arrangement	PCM [a]	PCM [b]	PCM [c]
Melting temperature (°C)	382.1	439.8	505
Solidification temperature (°C)	390.9	429.8	450.1
Latent heat of fusion (kJ·kg^{-1})	197.6	214.9	344
Latent heat of solidification (kJ·kg^{-1})	183.7	162.9	344
Solid density (kg·m^{-3})	2118	2109	2266
Liquid density (kg·m^{-3})	1607	1604	2160
Solid thermal conductivity (W·m^{-1}·K^{-1})	1.0	1.0	2
Liquid thermal conductivity (W·m^{-1}·K^{-1})	1.0	1.0	1.885
Solid specific heat capacity (J·kg^{-1}·K^{-1})	928	1005	1338.88
Liquid specific heat capacity (J·kg^{-1}·K^{-1})	1035	1096	1757.28

where
[a] 59.98 wt% $MgCl_2$-20.42% KCl-19.6% NaCl.
[b] 55 wt% $MgCl_2$-45%NaCl.
[c] 35 wt%Li_2CO_3-65 wt%K_2CO_3.

convection h_{out} on tank wall:

$$h_{out} = \frac{Nu_{out}k_w}{H} = \frac{\left[0.825 + 0.387[Ra\cdot f(Pr)]^{\frac{1}{6}}\right]^2 k_w}{H} \quad (13)$$

$$f(Pr) = \left[1 + (0.492/Pr)^{\frac{9}{16}}\right]^{\frac{16}{9}} \quad (14)$$

$$Ra = GrPr, \quad Gr = g\beta\Delta TH^3/\nu^2 \quad (15)$$

The coefficient of convective heat transfer h_{in} has been calculated from the following correlation [42]:

$$h_{in} = \left(\frac{k_f}{d_p}\right)\left(2.58Re_p^{1/3} + 0.094Re_p^{0.8}Pr^{0.4}\right) \quad (16)$$

Thermocline tank TES pressure drop for charge/discharge cycles is calculated based on equation from [43].

$$\Delta P = 150H\frac{(1-\varepsilon)^2}{\varepsilon^2}\frac{\mu_f u_f}{d_p^2} + 1.7H(1-\varepsilon)\frac{\rho_f u_f^2}{d_p} \quad (17)$$

2.2. PCM particles as filler materials

The process of phase transition inside the PCM(s) particles needs modeling of temperature based thermo-physical properties. It was calculated on three stages: solid, transition and liquid phase. If the temperature inside the PCM(s) particles is less or greater than this temperature difference ($T_{p2} - T_{p1}$), the storage or release energy is calculated as a sensible heat. Thermal conductivity of the PCM(s) particles for charge/discharge cycles is given as follows in phase transition:

(1) For PCM in the solid phase

$$If \quad T_p < T_{p1} \; c_p = c_{p,s} \quad \& \quad LF = 0 \quad k = k_s \quad (18)$$

(2) For PCM in the transition phase

$$If \; T_{p1} < T_p < T_{p2} \; c_p = c_{p,app} \; k = \frac{k_s + k_l}{2} \quad (19)$$

$$c_{p,app} = \frac{c_{p,s} + c_{p,l}}{2} + \frac{h_{fs}}{T_{p2} - T_{p1}} \quad (20)$$

(3) For PCM in the liquid phase

$$If \quad T_p > T_{p2} \quad c_p = c_{p,l} \quad \& \quad LF = 1 \quad k = k_l \quad (21)$$

2.3. Initial and boundary conditions

Initial conditions need only to be defined for the first cycle, after that, the initial values of the solid and fluid temperatures for each subsequent cycle during discharging cycle will be equal to those at the end of the charge cycle. The boundary conditions are defined for the heat transfer fluid at the inlet and the outlet, where the temperature is continuously measured. To make the analysis more simplistic and reduce numerical time, PCM(s) particles are supposed to be isotropic, and there is no change in the overall porosity of the tank, which means the HTF temperature and mass flow rate are uniformly changed through the porous structure. Therefore, it can be said that the system is designed on a one-dimensional model. From the above-mentioned assumptions,

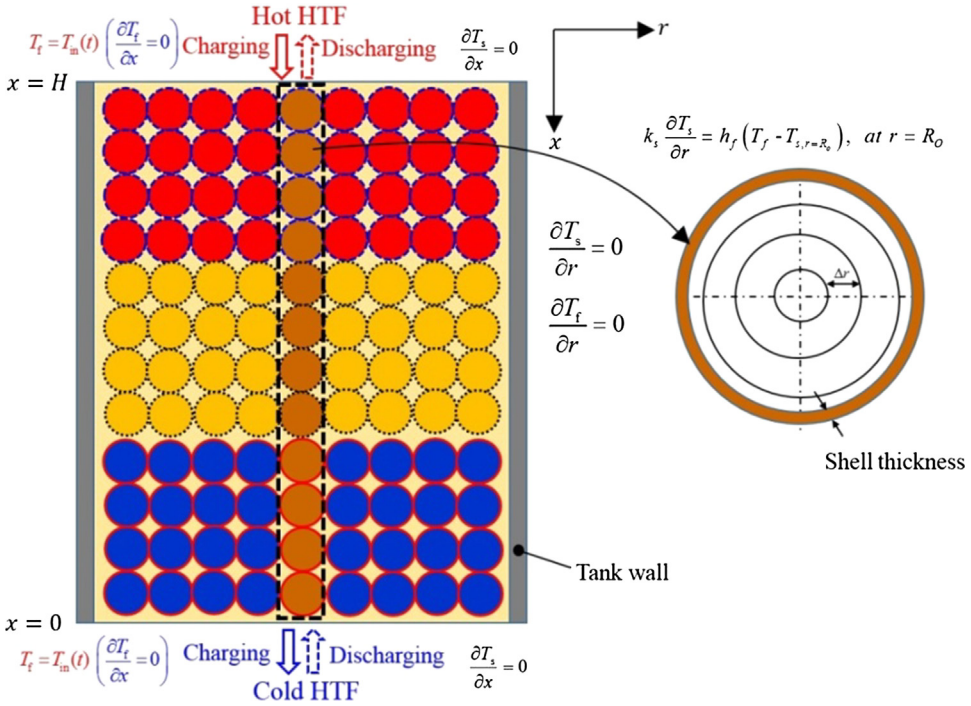

Fig. 2. Boundary conditions for (D-C) heat transfer model.

the energy equation has been calculated for each PCM particle in axial direction over thermocline tank height, after that, the temperatures distributions for all other PCM(s) particles at the same axial position have been represented simultaneously by the same method. By using the discretization method, each PCM particle has been modeled as axisymmetric and discretized into equal spaces in the radial direction. The initial and the boundary conditions for the HTF and PCM(s) particles during charging discharging cycles are shown in Fig. 2.

2.4. Heat exchange zone

The storage process in the tank is described by different basic thermocline regions over the height of the tank as presented in Fig. 3. At the beginning of the charge cycle, the HTF passes through the inlet of thermocline tank and fills the packing area. Because of this, the energy exchange occurs between HTF and PCM(s) particles that lead to create a heat transfer region which can be called thermocline zone. This zone moves down along the tank during the charge cycle, leaving behind a high temperature zone and at the same time leads to increase the temperature of the zone below it. Therefore, the hot and cold regions can be defined as the upper and lower part of the tank, respectively. During discharge cycle, the HTF and thermocline zone proceed from bottom of the tank to the top. The hot and cold zones mixing of the thermocline tank can be preserved by a density gradient resulting from the temperature difference between them which creates buoyancy forces. The operational efficiency of the thermocline tank TES system can be enhanced by placing PCM(s) particles with low melting temperature at the lower part of the tank for charge cycle and make the HTF temperature at the exit of the tank constant for discharge cycle. As a result of high levels of mixing between the hot and cold zones leads to loss of exergy inside the tank. Also, this allows HTF to be exited from the tank at high temperatures without any utilization [44].

However, in actual CSP plants, the charge/discharge cycles is not necessary determined over a specified period of time, but are determined based on maximum and minimum cut off temperature for charge/discharge cycles, respectively. In charge/discharge cycles, the thermocline zone reaches the lower or the upper part of the thermocline tank, yet this depends on the thermo-physical properties of the PCM(s) particles chosen because, when the PCM(s) particles have a high heat capacity, it may need much longer time. The heat capacity of the PCM (s) particles strongly affects the time required to complete charge/discharge cycles. Thermocline zone could be described by the propagation velocity, $v_{t,sens}$, which is defined as follows:

$$v_{t,sens} = \frac{c_{p,f}\rho_f u_f}{\varepsilon c_{p,f}\rho_f + (1-\varepsilon)c_{p,s}\rho_s} \tag{22}$$

It depends on the thermo-physical properties of PCM(s) particles, HTF properties and the porosity of the thermocline tank. For the charge/discharge cycles, the time will be t_o, therefore, the distance that the HTF will travel is equal to ($v_{t,sens} * t_o$). The value of this distance shows the length which the HTF travels over a certain period of time and at the same time gives the tank height required during the charge/discharge cycles. To reach the ideal state, the value of $v_{t,sens}$ must be less than the tank height. If the value of $v_{t,sens}$ is greater than the tank height, the charge cycle of the tank will complete before the charge period ends and the storage capacity will be ended before the discharge cycle is complete.

The effects of two parametric studies (inverse Stefan number and dimensionless temperature difference) on the thermal performance depend on the sensible heat propagation velocity and the phase change in the thermocline zone, defined by Eq. (22). The phase change propagation velocity for the charge cycle is determined from the following equation as discussed by Fleuckiger et al. [22]:

$$v_{latent,ch} = \frac{c_{p,f}\rho_f u_f}{\varepsilon c_{p,f}\rho_f + (1-\varepsilon)c_{p,s}\rho_s\left[1 + \frac{1}{Ste}\left(\frac{T_{h,f}-T_{c,f}}{T_{h,f}-T_{p1}}\right)\right]} \tag{23}$$

and for the cycle of discharge as:

$$v_{latent,disch} = \frac{c_{p,f}\rho_f u_f}{\varepsilon c_{p,f}\rho_f + (1-\varepsilon)c_{p,s}\rho_s\left[1 + \frac{1}{Ste}\left(\frac{T_{h,f}-T_{c,f}}{T_{p2}-T_{c,f}}\right)\right]} \tag{24}$$

Eqs. (23) and (24) show that phase change propagation velocity depends on the melting temperature and latent heat of the PCM(s) particles. For charge/discharge cycles, the travel rate of the phase transition propagation velocity will be fast with a decrease in the latent heat value of the PCM(s) particles or by increasing the temperature difference between the charge HTF and PCM(s) particles.

2.5. Parametric study

The thermal performance of the thermocline tank is discussed by two parametric studies (inverse Stefan number and dimensionless

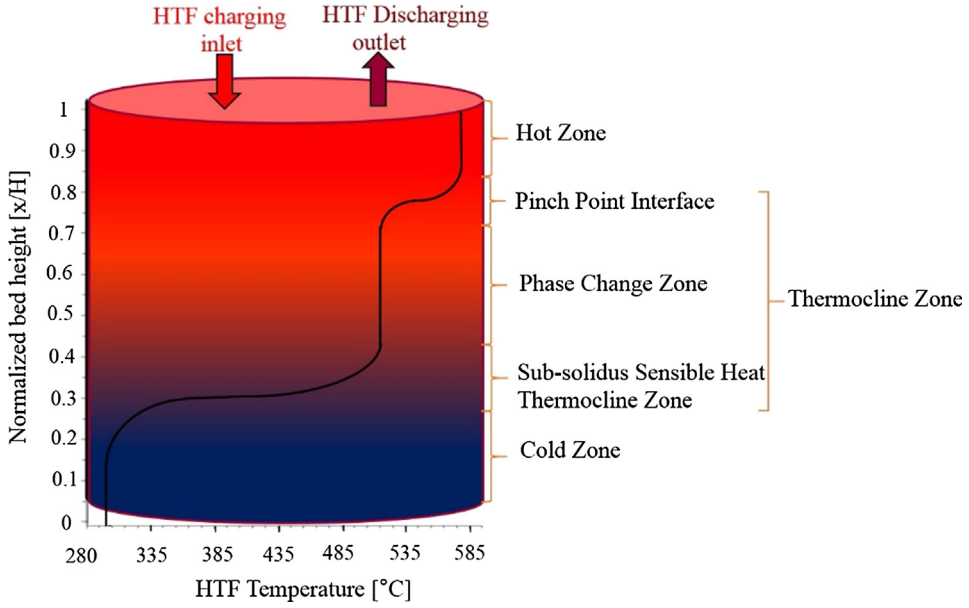

Fig. 3. Progression of the different zones of the thermocline tank during the charge/discharge cycles.

temperature difference) [22]. These two parametric studies have been used to identify the optimum values of latent heat and melting temperature for MLPCM(s) that could maximize the output energy from the storage system. By using these parameters, the values of the latent heat and melting temperature for MLPCM(s) are changed either in the top, middle or bottom section of the thermocline tank. The latent heat magnitude inside the PCM(s) particles is defined as the ratio of latent heat to sensible heat (inverse Stefan number):

$$InvSte = \frac{h_{fs}}{c_{p,ave}(T_{h,f} - T_{c,f})} \quad (25)$$

The magnitude of the melting temperature (dimensionless temperature difference) inside the PCM(s) particles is expressed as:

$$\theta = \frac{T_p - T_{c,f}}{T_{h,f} - T_{c,f}} \quad (26)$$

where $T_{h,f}$ and $T_{c,f}$ are the HTF inlet temperature during charge/discharge, respectively.

The above two parametric studies determines the influence of latent heat and melting temperature on the thermal performance of the thermocline tank and the energy output from MLPCM(s) for all cases studied. Table 3 shows the values of the *InvSte* number and the dimensionless temperature for all cases studied.

2.6. Numerical approach

The thermocline tank has been divided into equal number of control units (CV_s) with discretization of the axial direction into equal number of parts N_x and the radial direction into equal number of parts R_x for all the cases studied including the numerical model validations as shown in Fig. 2. The process of heat exchange between filler materials and HTF is the same as between PCM(s) particles and HTF per unit volume. By direct approximation of finite differences method within the full implicit approach, the governing equations of the numerical model have been solved in MATLAB. The method of First order upwind approach has been applied to divide both of the temporal and advective terms as in Eq. (5), at the same time; second order central difference approximation has been applied to divide the diffusion term. Initially, the HTF temperature distribution and the PCM(s) particles are solved by using the boundary condition after that these equations are simultaneously solved as shown in Fig. 2. At each time step, the thermo-physical properties of PCM(s) particles and HTF temperature distribution are updated.

All the study cases have been compared based on operating conditions defined in Table 1. The mass flux of HTF is constant during charge/discharge cycles to decrease the influence of dissimilar convective heat transfer rates, as shown in Table 1. After completing the study of the division and specifying the time step size, the thermocline tank has been divided into equal part 0.0245 m in the axial direction and the time step size has been selected as 1 s. For the discretization of the PCM(s) particles, each particle has been divided into 30 equal parts in the radial direction. To calculate the difference in temperature between PCM(s) particles and HTF at each part during charge/discharge cycles, the volume averaged method is applied.

3. Performance analysis

3.1. Energy efficiency

The efficiency of charge cycle is determined as the ratio between the stored energy in the PCM(s) particles and the HTF inside the thermocline tank to the input and pumping energy after reaching the steady state [45]:

$$\eta_{ch} = \frac{E_{stored}}{E_{input} + E_{pump,ch}} \quad (27)$$

The efficiency of discharge cycle is determined as the ratio of energy output from the thermocline tank to stored and pumping energy:

$$\eta_{disch} = \frac{E_{outflow}}{E_{stored} + E_{pump,disch}} \quad (28)$$

The overall efficiency of the cycle of the thermocline tank TES tank is the ratio between the output energy to the input and total pumping energy for charging and discharging cycles [46].

$$E_{pump} = \int_0^{t_{end}} \frac{\dot{m}}{\rho_{HTF}} \Delta P dt \quad (29)$$

$$E_{stored} = E_{stored\ after\ ch} - E_{stored\ before\ ch} \quad (30)$$

$$\eta_{overall} = \frac{E_{outflow}}{E_{input} + E_{pump,ch} + E_{pump,disch}} \quad (31)$$

3.2. Capacity ratio

Capacity ratio is defined as the ratio of stored energy to the maximum energy stored for the charge cycle.

$$\sigma = \frac{E_{stored}}{E_{stored}^{max}} \quad (32)$$

The energy stored inside each PCM(s) particle is calculated by knowing the state of PCM if it is in solid phase, liquid phase, or phase change. The phase change temperatures range of PCM(s) particles used are shown in Table 2. The liquid fraction can be determined as follows:

$$LF = \frac{T_p - T_{p1}}{T_{p2} - T_{p1}} \quad (33)$$

3.3. Utilization ratio

Utilization ratio is defined as the ratio between the amount of energy that can be released to the maximum energy stored for the charge cycle [46].

$$\gamma = \frac{E_{disch}}{E_{stored}^{max}} \quad (34)$$

The discharged energy has been calculated based on the difference between the energy stored for charge cycle and the energy remaining in the PCM(s) particles and the HTF after the discharge cycle:

$$E_{disch} = E_{stored\ after\ ch} - E_{stored\ after\ disch} \quad (35)$$

The maximum possible energy that can be stored in the system is calculated as:

$$E_{stored}^{max} = m_{PCM} c_{p,l}(T_{inlet} - T_{p2)}) + m_{PCM} h_{fs} + m_{PCM} c_{p,s}(T_{p1} - T_{PCM,initial}) \quad (36)$$

Table 3
Cases summary of ML PCM(s) configurations.

Case	Bottom PCM	Middle PCM	Top PCM
Case A: Base Case	*InvSte* = 0.7 (θ_m = 0.35)	*InvSte* = 0.75 (θ_m = 0.55)	*InvSte* = 1.2 (θ_m = 0.8)
Case B	*InvSte* = 0.65 (θ_m = 0.3)	*InvSte* = 0.75 (θ_m = 0.55)	*InvSte* = 1.2 (θ_m = 0.8)
Case C	*InvSte* = 0.75 (θ_m = 0.4)	*InvSte* = 0.75 (θ_m = 0.55)	*InvSte* = 1.2 (θ_m = 0.8)
Case D	*InvSte* = 0.7 (θ_m = 0.35)	*InvSte* = 0.7 (θ_m = 0. 5)	*InvSte* = 1.2 (θ_m = 0.8)
Case E	*InvSte* = 0.7 (θ_m = 0.35)	*InvSte* = 0.8 (θ_m = 0.6)	*InvSte* = 1.2 (θ_m = 0.8)
Case F	*InvSte* = 0.7 (θ_m = 0.35)	*InvSte* = 0.75 (θ_m = 0.55)	*InvSte* = 1.15 (θ_m = 0.75)
Case G	*InvSte* = 0.7 (θ_m = 0.35)	*InvSte* = 0.75 (θ_m = 0.55)	*InvSte* = 1.25 (θ_m = 0.85)

4. Results and discussion

4.1. Model validation

The numerical study is validated against the experimental data as published by Pacheco et al. [47]. The molten salt has been used as the heat transfer fluid. In Fig. 4, the present numerical model (solid line) is compared to Pacheco et al. experimental data (dash line). The change in temperature of the HTF for the experimental data occurs at different heights because of the high levels of mixing between the different zones during charge. The average deviation between the present numerical model and experimental results were approximately 4.32% of the change in temperature over the thermocline TES tank height. The results obtained from the current numerical study are consistent with the experimental results. After the results verification, it can be confirmed that the results obtained from this study is reasonable.

4.2. Temperature distributions in thermocline tank

Fig. 5 shows the HTF axial temperature distribution over the height of the tank during the charge cycle for the all study cases. Clearly, the thermal performance of the thermocline tank is influenced by the configurations of PCM(s) particles inside it. Inspection of Eq. (23) reveals that the phase change propagation velocity travel rate is dependent on the heat of fusion (non-dimensionalized as the *InvSte*) and the melting temperature during charge cycle for the PCM(s) particles. During charge cycle, the travel rate of the phase change propagation velocity will be slower when the latent heat value is high or when the temperature difference between the HTF and PCM(s) particles is low. Eq. (22) determines the travel rate of the subsolidus sensible heat thermocline zone while the travel rate of the phase transition propagation velocity can be determined by Eq. (23). The rate of travel of the phase change zone restricts the movement of hot zone, thus not progressing deep into the thermocline tank. Fig. 5 indicates the travel rate of each zone during the charge cycle for all the study cases. After completion of tank charging, the zone of the thermocline reached the lower section of the tank, the phase transition zone enlarged, and the hot zone greatly extended. From the Fig. 5, the case (B) is the fastest to melt because of the phase change propagation velocity moves at a rate 0.96 of times the HTF velocity, followed by case (A), the travel rate is 0.90 times the HTF velocity while, for case (C), the rate of travel is only 0.35 times the HTF velocity.

Fig. 6 shows the HTF axial temperature distribution over the thermocline tank during the discharge cycle for all cases studied. During discharge cycle, the high solidifying temperature will increase the heat transfer rate between the PCM(s) particles and the HTF. The phase change propagation velocity with high solidifying temperature will correspond closely with the travel rate of sub-sensible heat thermocline zone. The rate of heat transfer will decrease not only with the increase of latent heat, but also with the reduction of difference between the PCM(s) particles temperature and the HTF discharge temperature as shown in Eq. (24).

For the discharge cycle, the HTF exits of the thermocline TES tank at the solidification temperature of the PCM(s) particles for a certain period of time. This will increase the HTF exit temperature and it will be higher than the temperature of the PCM(s) particles, which has lower phase change temperature. This can be explained as follows: If the thermocline tank is filled with PCM(s) particles with low melting temperature, the full heat capacity of these PCM(s) materials can be utilized during the charge cycle, but the opposite happens during the discharge cycle, the extracted energy is gradually reduced because the heat transfer rate is slow. For this reason, this system suffers from unwanted influences that prevent the benefit of utilizing maximum storage energy and maximum use of stored energy at the same time.

The case (B) is the fastest to solidify, the discharging solidifies moves at a rate of 0.92 times the rate of travel of the HTF, followed by case (A) in which the rate of travel is 0.85 times the HTF velocity while, for case (C), the rate of travel is only 0.31 times the HTF velocity. The rate of heat transfer increases as the difference in temperature between the PCM(s) particles and the HTF increases. The solidifying cycle will be very slow whenever the solidifying temperature of the PCM(s) particles is too close to the HTF temperature. In case (B), the distribution of the solidifying temperature corresponds to the temperature of the HTF much better. By the end of discharge cycle, the case (B) has achieved the maximum amount of stored energy that can be recovered as compared to all the other study cases. Due to the high amount of energy recovered from the system by the end of the discharge cycle and quickly arriving at steady state. For these reasons this is almost the best scenario where the thermocline TES tank can store and recover maximum storage capacity of the PCM(s) particles.

Fig. 7 presents the HTF temperature distribution for all cases studied at different height for charging cycle. The figure illustrates the benefit of the MLPCM(s). The latent heat value affects the thermocline TES tank efficiency, which have a common influence on the thermal performance during charge/discharge cycles. During the charge cycle, the bottom and the middle PCM(s) particles serves as a buffer and this allows the system to store more energy. The case (B) presents the highest level of performance, and case (C) shows the lowest level of performance. As explained in the previous paragraphs, for case (B), the top PCM particles melt is completed before the collapse of the pinch point interface and allow the hot zone to move to the lower part of the tank. Also, the PCM particles that exist in the bottom of the tank work as buffer to limits the saturation state. This allows the tank to extend the charge period for the longest possible period of time and release more stored energy with higher efficiency. For this reason, the highest energy output can be obtained from case (B).

Fig. 8 shows the temperature distribution over time at different height for discharge cycle. The temperature distribution of cases (B) and (G) are nearly identical. The two cases (B) and (D) have the highest heat of fusion in the bottom and middle sections of the tank, respectively. These two cases showed the highest capacity ratio, but they are unable to fully discharge the storage energy, as shown in the final form of the discharge cycle in Fig. 8. The case (G) has high latent heat at the top section of the tank, so, it's unable to reach the hot inlet temperature of the HTF. When the highest latent heat value is in the middle and bottom sections of the tank as in case (E), the system performance is equivalent to the condition in case (C) in which the lower section only contains high heat of fusion. During the charge/discharge cycles for all cases studied, case (B) presents an optimized performance which is fully consistent with previous conclusions.

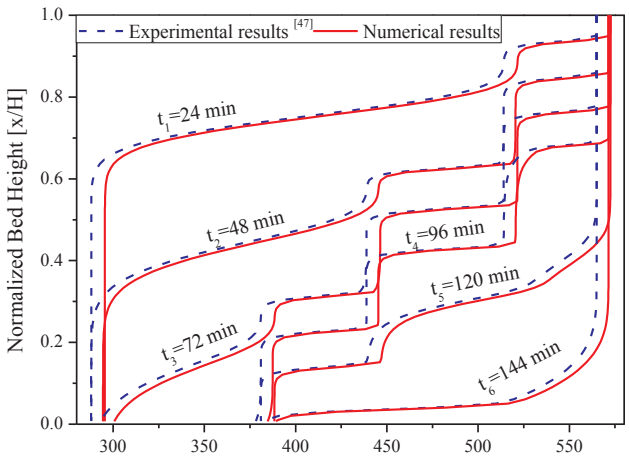

Fig. 4. Comparison between current numerical result of axial HTF temperature distribution in thermocline tank and experimental results from Pacheco et al. [47]

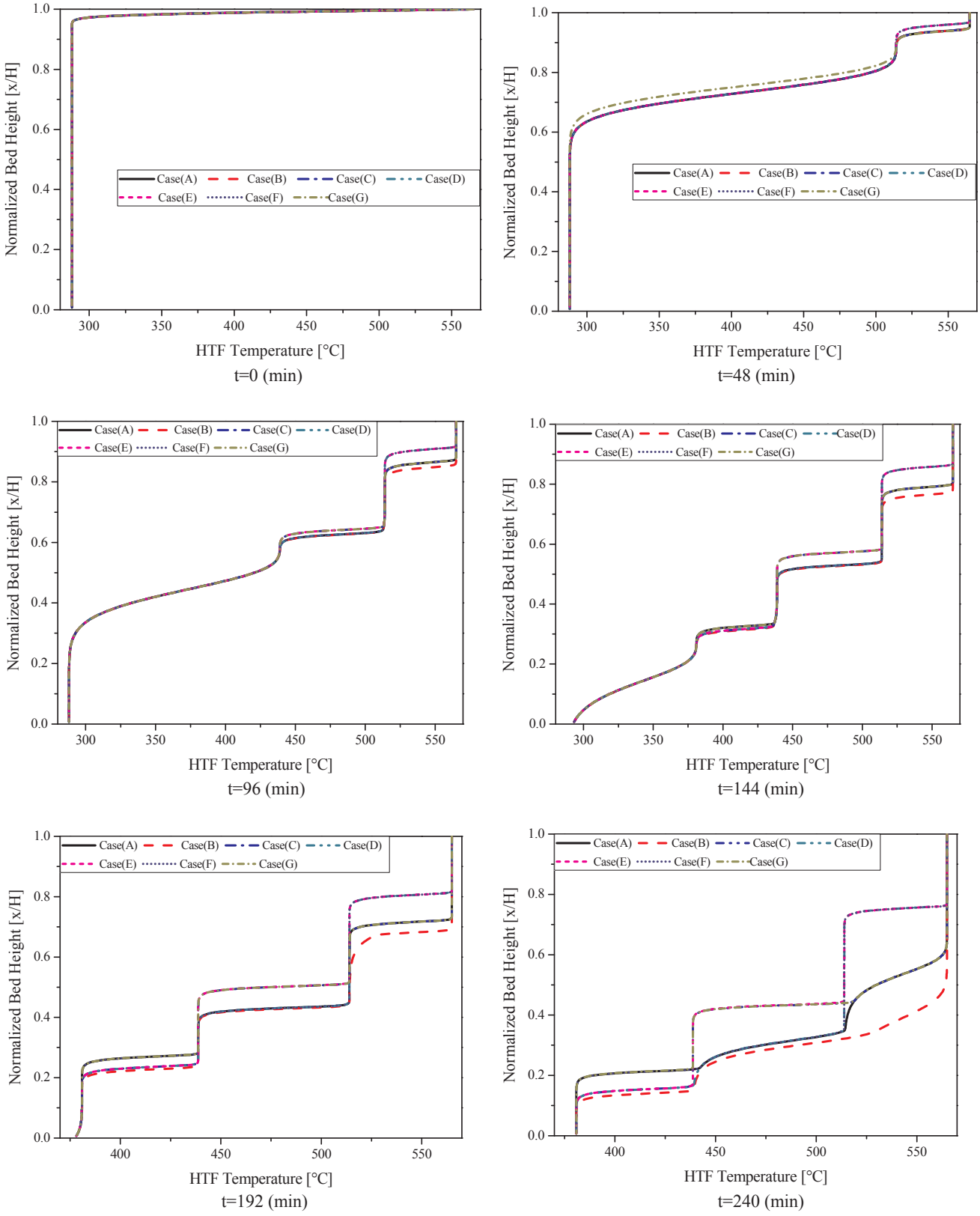

Fig. 5. HTF axial temperature distribution over height at different time for charge cycle.

Fig. 9a and b provides the corresponding PCM(s) particles temperature distribution over the thermocline tank after reaching the steady state during the charge/discharge cycles, respectively. The system takes 350 min to reach the steady state; during this cycle the system stored 96.7% of its maximum storage capacity, which is equal to 97.8 kWh. The discharging cycle is completed in 320 min and during this cycle 86.16% of the stored energy is recovered, which is equal to 87.5 kWh. Table 3 provides the characteristics of all the studied cases, which have the highest latent heat and melting temperature either at the bottom, middle or top of the packed bed. The case (C), which has

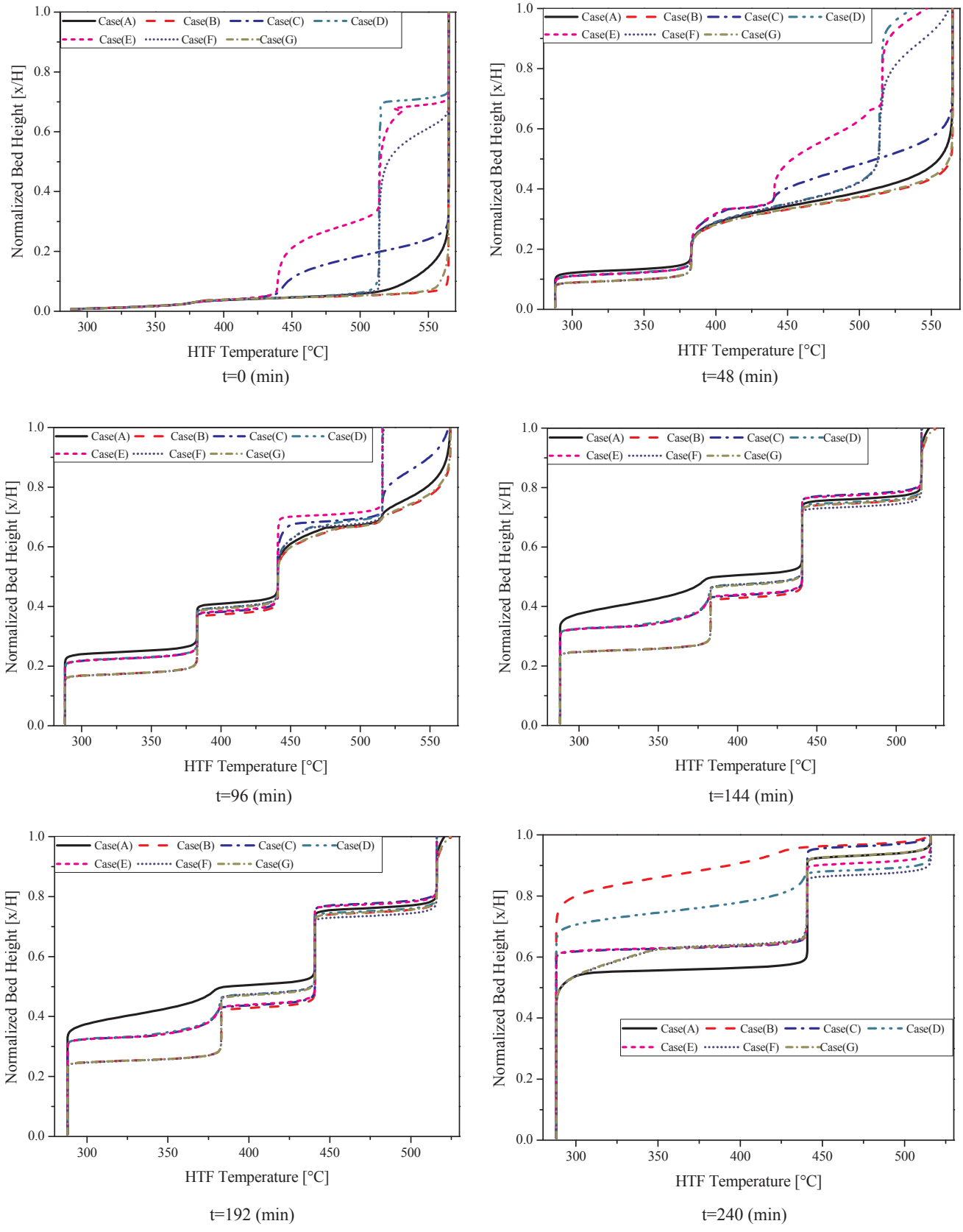

Fig. 6. HTF axial temperature distribution over height at different time for discharging cycle.

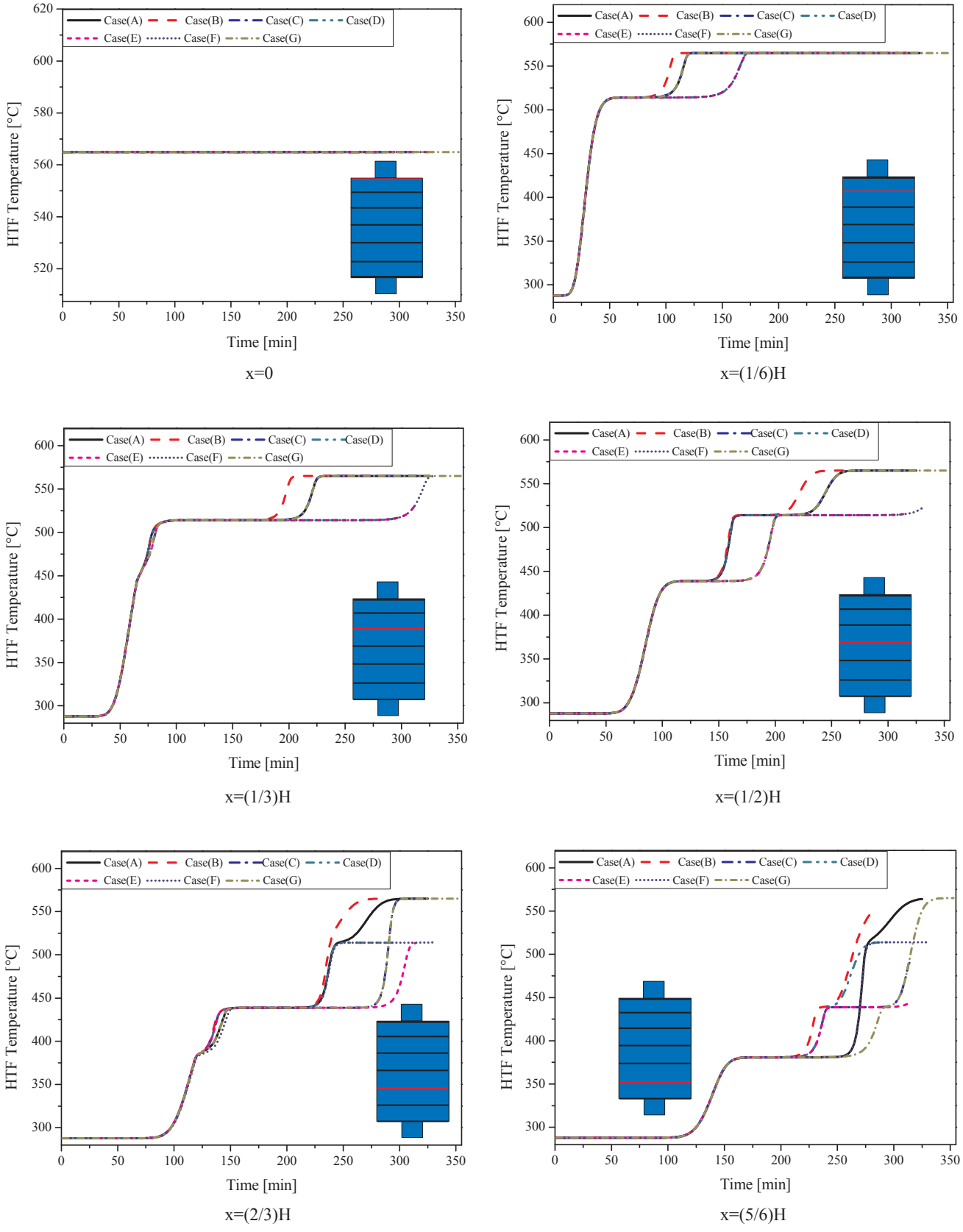

Fig. 7. HTF axial temperature distribution over time at different height for charging cycle.

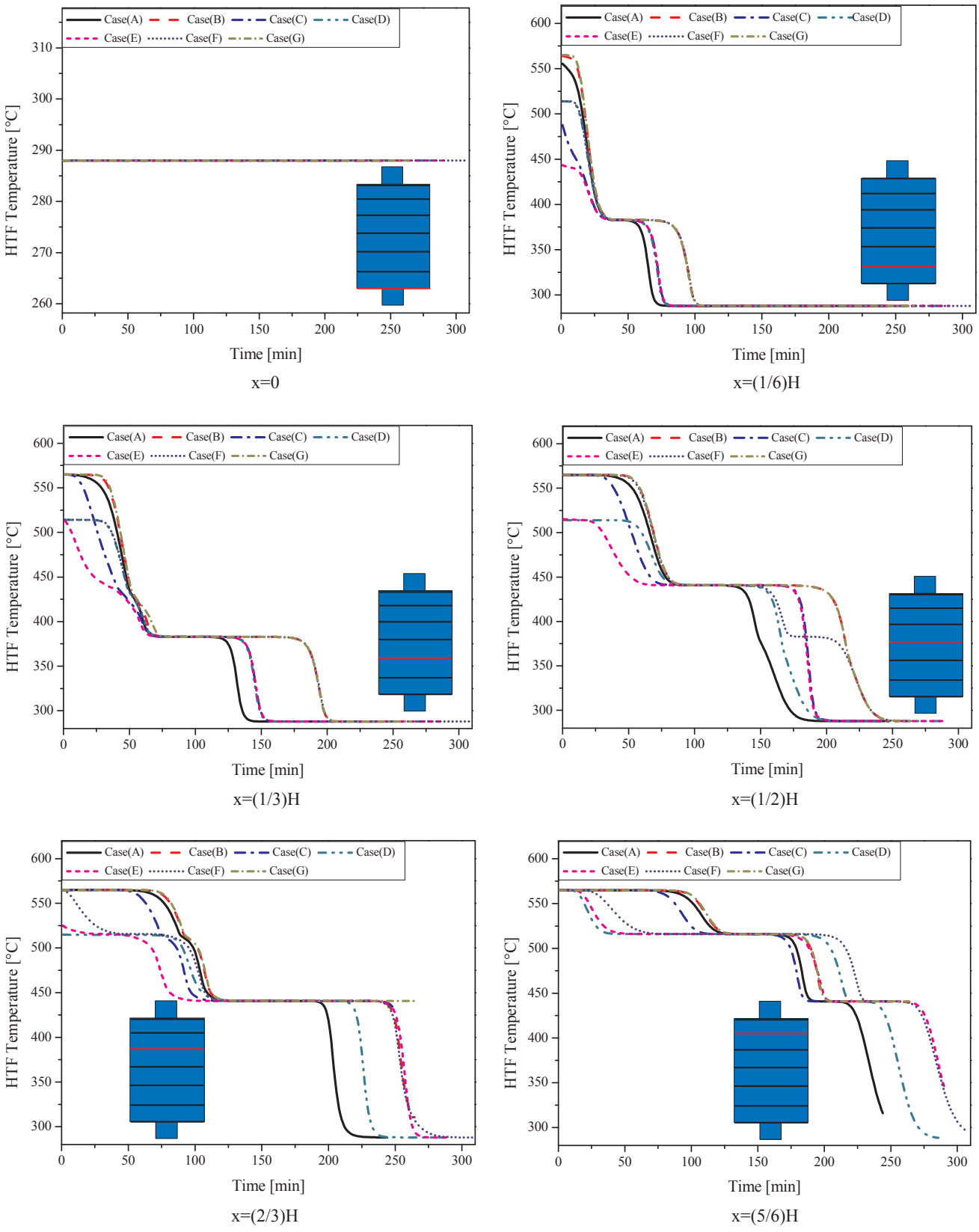

Fig. 8. HTF axial temperature distribution over time at different height for discharging cycle.

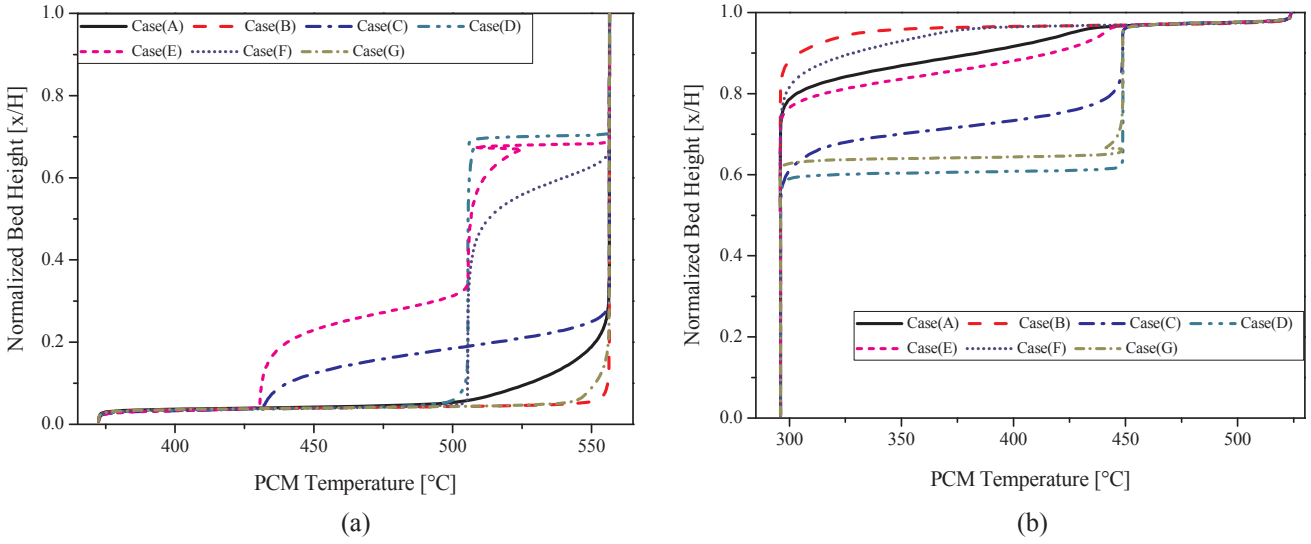

Fig. 9. Steady state PCM(s) temperature distribution for (a) charge (b) discharge cycle.

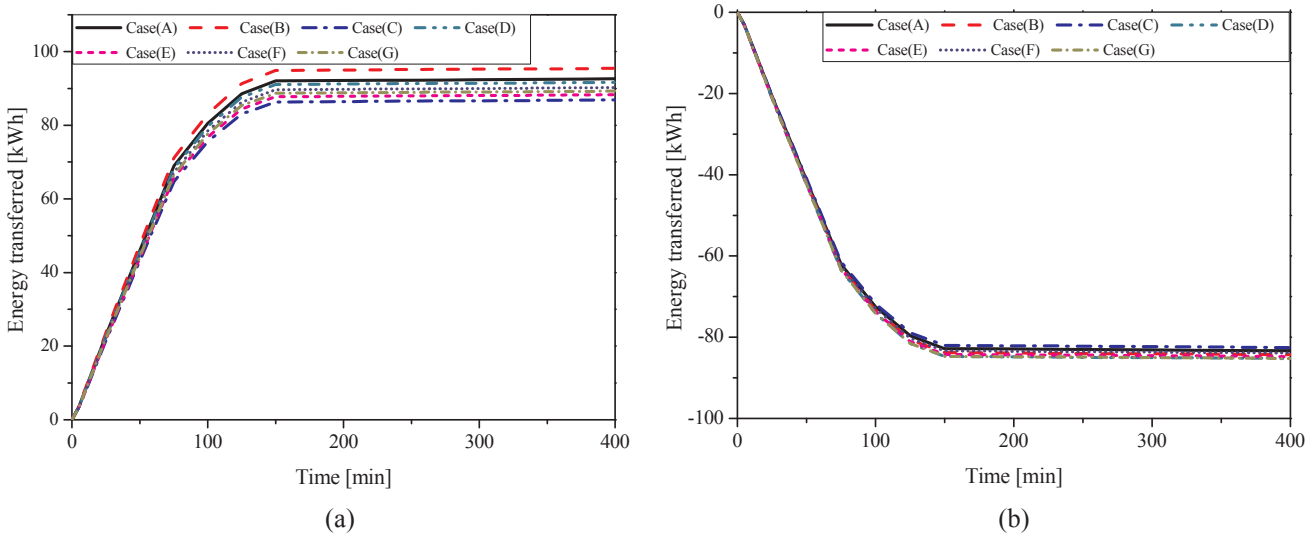

Fig. 10. Total energy transferred to and from bed for (a) charging (b) discharge cycles respectively.

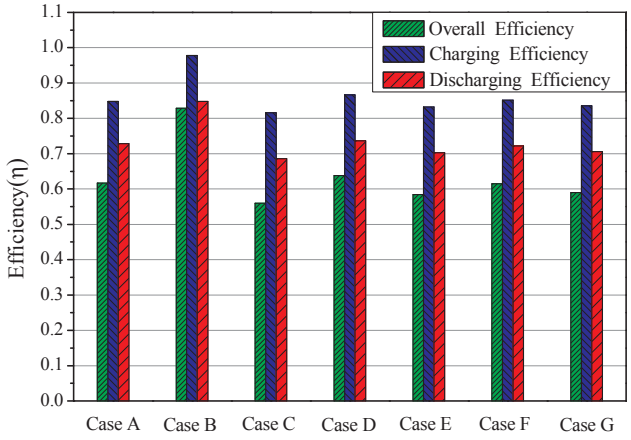

Fig. 11. The performance parameters of the thermocline tank TES system for energy efficiency.

the highest latent heat at bottom, requires the largest time for the discharge cycle, thus less amount of energy can be recovered as shown in Fig. 11. The blow assessment is used as a theory to understand the effect of heat of fusion (*InvSte*) and melting temperature (dimensionless temperature difference) on the performance of MLPCM(s) thermocline tank under the assigned parametric combination.

For the charge cycle, case (B) is one of the fastest cases that happen to have a completely melting, because of the matching in temperature distribution between the PCM(s) particles and the HTF; case (G) comes second in the order. Also, for the discharge cycle, case (B) is the fastest case that happens to be solidified, because case (B) showed the lowest distribution of temperature; this means that the maximum possible amount of energy that was stored during the charge cycle has been recovered. The above stated discussion provides the reasons why this design has a better performance during charge/discharge cycles.

4.3. Storage capacity

The following study explores the thermal performance of all the studied cases for thermocline tank in terms of the total energy stored both during the charge/discharge cycles as shown in Fig. 10a and b,

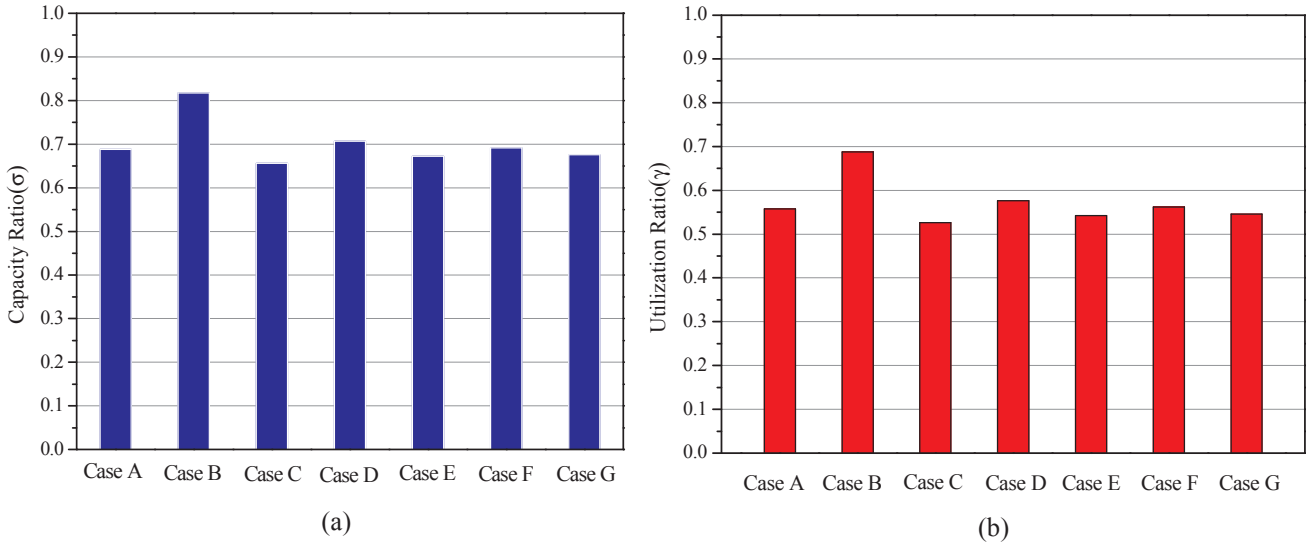

Fig. 12. The performance parameters of the thermocline tank TES system (a) capacity ratio (b) utilization ratio.

respectively. The rate of heat transfer between PCM(s) particles and HTF measures the tank storage capacity, and the large temperature difference between them indicates that a big force required to increase the heat transfer process, which will enhances pinch point interface zone movement. Because of the melting temperature in the top PCM(s) particles is high as in case (G), this caused the movement of the pinch point interface to be slow, thus limiting the growth of the hot zone. Although, the case (B) system design showed its potential to store as much energy as possible, it can't fully recover this stored energy because of the restrictions on the process of heat transfer caused by the phenomenon of pinch point interface. The case (B) system design can provide more storage capacity than the other studied cases with the same tank size. Fig. 10a shows the thermal performance of the all studied cases for charge cycle as function of the overall energy that has been stored. The case (B) provides the highest thermal performance, following by the cases (A and D) and case (C) is the worst in all cases studied. Also, the case (B) has the highest heat transfer rate, because this design has a better melting temperature distribution consistent with the temperature of HTF. In the rest cases, performance is lower due to lower heat transfer rate between PCM(s) particles and HTF.

The thermal performance of the thermocline tank is shown in Fig. 10b for discharging cycle as function of the total energy that has been recovered from the storage system. In the current study, the case (B) achieved the highest thermal performance. The lowest thermal performance was achieved by the other two the cases (E, C). This is due to the driving force existing in heat flow, which has a strong relationship with the difference in temperature between the PCM(s) particles and the HTF. After analyzing the performance of the all cases for the charge/discharge cycles, the only design that showed the highest possible thermal performance is the case (B) design.

4.4. Performance parameters

Different parameters have been presented in the performance analysis part to determine the optimal thermal performance of thermocline tank and to investigate all the study cases. Energy efficiency is one of the measures applied in the current study to express the quantity and quality of energy that has been stored and released from the storage tank for charge/discharge cycles. The energy efficiency, capacity ratio and utilization ratio are applied to study and understand the thermal performance of the thermocline tank.

Thermocline TES tank suffer from large discrepancies between the PCM(s) particles thermodynamic properties and HTF temperature during charge/discharge cycles as shown in Fig. 11. High melting temperatures can give high TES during charge cycle, but the large discrepancy in the rate of travel between the HTF and the PCM(s) particles leads to less charging efficiency. Although, if PCM(s) particles with low melting temperatures are used, this will lead to fully utilization of the capacity of the PCM(s) particles for charging cycle but can't get high TES. The variation in the performance of thermocline TES tank for all the study cases is explained by varying the latent heat and the melting temperature of the MLSPCM.

The thermal performance for all the studied cases as a function of efficiency has been presented in Fig. 11. The case (B) configuration shows the higher thermal performance, case (A) is the second case in terms of thermal performance and case (C) is the least case. It is shown that energy efficiency varies between 83.6% and 55.76, for all the cases.

Fig. 12 show the capacity ratio and the utilization ratio for the thermocline tank during charge/discharge cycles, respectively. The magnitude of the storage capacity in the tank is variable and dependent on the heat of fusion and the melting temperature of PCM(s) particles. Fig. 12a shows the capacity ratio of thermocline tank TES system. The case (C) structure exhibits the lowest capacity ratio of 0.645. The highest value is observed in case (B), which showed a capacity ratio equal to 0.818. Fig. 12b shows the utilization ratio of thermocline tank TES system. The largest gains are observed with the case (B), which exhibits the utilization ratio of 0.689. The case (C) structure exhibits the lowest utilization ratio of 0.525. The closer the melting temperatures of the MLPCM(s) for all the study cases to the average temperature of the HTF, the greater rates of latent heat exchange for the charge (Eq. (23)) and discharge (Eq. (24)) cycle. Whereas this compatibility is desirable, the melting temperatures of the upper and lower of the MLPCM(s) particles should stay out the HTF thermal dead zone to maintain temperature difference in order to prevent the choking phenomenon as discussed previously in Section 2.4. Therefore, an optimal MLPCM(s) configuration should have a top PCM layer that melts slightly below the HTF charge inlet temperature and a bottom PCM layer that solidifies slightly above the HTF discharge inlet temperature.

5. Conclusions

A transient (D-C) numerical model for LHTES thermocline tank using PCM capsules is used in the current study to investigate the thermal performance of seven cases of MLPCM(s). Thermal performance of these cases are analyzed by studying the axial HTF

temperature distribution, the sensible heat propagation velocity, the phase change in thermocline zone, the quantity and quality of energy that can be stored and released from the thermocline tank. Moreover, two parametric studies have been used to determine the optimal values of melting temperature and heat of fusion for these cases that would increase the energy storage and recovery from the storage system. The storage capacity, overall thermal efficiency, utilization ratio and capacity ratio are investigated based on these parameters. From the analysis conducted in the current study, the important results obtained can be summarized as follows:

(1) In this study, the thermal performance of the LHTES thermocline tank system can be successfully verified using a transient (D-C) numerical model taking into account the radial heat transfer and wall heat losses.
(2) The MLPCM(s) case (B) configuration has a much higher heat transfer rate than the all other studied cases during charging/discharging cycles. Because the best match in temperature distribution between PCM layers and HTF appeared in this case.
(3) In the optimal configuration of the case (B), the values of *InvSte* number and dimensionless temperature (θ) are equal to 1.2 and 0.8 for the top PCM layer, respectively; 0.75 and 0.55 for the middle PCM layer, respectively; and 0.65 and 0.3 for the bottom PCM layer, respectively.
(4) To obtain the best design and distribution of temperature for a thermocline tank TES tank consisting of three layers of PCM, the top PCM layer should melts by $\Delta T = 55.4$ °C below the HTF charging inlet temperature ,the PCM layer at the bottom should solidifies by $\Delta T = 83.1$ °C above HTF discharging inlet temperature.

According to the above conclusion, the MLPCM(s) case (B) can be used for a thermocline tank LHTES system for CSP plants at night time when there is no sunshine and demand for electricity is in peak condition. Because the MLPCM(s) case (B) is advantageous in improving the charging/discharging rate and the thermal performance in comparison with all the other studied cases therefore, the integration of MLPCM(s) case (B) with CSP plants is capable of making the grid load more stable and decreasing more running fee. In addition, the optimization results that have been obtained can be served as reference guidance for designers in the CSP plants sector.

Acknowledgments

This work is financially supported by the National Natural Science Foundation of China (Grant No. 51536007), the National Natural Science Foundation of China (NSFC)/Research Grants Council (RGC) Joint Research Scheme (Grant No. 51861165105), the Foundation for Innovative Research Groups of the National Natural Science Foundation of China (No.51721004), the 111 Project (B16038) and the Fundamental Research Funds for the Central Universities (xjj2018199).

References

[1] Pelay U, Luo L, Fan Y, Stitou D, Rood M. Thermal energy storage systems for concentrated solar power plants. Renew Sustain Energy Rev 2017;79:82–100.
[2] Kuravi S, Trahan J, Goswami DY, Rahman MM, Stefanakos EK. Thermal energy storage technologies and systems for concentrating solar power plants. Prog Energy Combust Sci 2013;39:285–319.
[3] Bruch A, Molina S, Esence T, Fourmigué JF, Couturier R. Experimental investigation of cycling behaviour of pilot-scale thermal oil packed-bed thermal storage system. Renew Energy 2017;103:277–85.
[4] Zanganeh G, Khanna R, Walser C, Pedretti A, Haselbacher A, Steinfeld A. Experimental and numerical investigation of combined sensible-latent heat for thermal energy storage at 575°C and above. Sol Energy 2015;114:77–90.
[5] Mahmood M, Traverso A, Traverso AN, Massardo AF, Marsano D, Cravero C. Thermal energy storage for CSP hybrid gas turbine systems: dynamic modeling and experimental validation. Appl Energy 2018;212:1240–51.
[6] Pirasacia T, Wickramaratnea C, Moloneya F, Goswamia DY, Stefanakosa E. Influence of design on performance of a latent heat storage system at high temperatures. Appl Energy 2018;224:220–9.
[7] Xu B, Li P, Chan C. Application of phase change materials for thermal energy storage in concentrated solar thermal power plants: a review to recent developments. Appl Energy 2015;160:286–307.
[8] Elfeky KE, Ahmed N, Wang QW. Numerical comparison between single PCM and multi-stage PCM based high temperature thermal energy storage for CSP tower plants. Appl Therm Eng 2018;139:609–22.
[9] Sunku Prasada J, Muthukumara P, Anandalakshmib R, Niyasa H. Comparative study of phase change phenomenon in high temperature cascade latent heat energy storage system using conduction and conduction-convection models. Sol Energy 2018;176:627–37.
[10] Liu M, Saman W, Bruno F. Review on storage materials and thermal performance enhancement techniques for high temperature phase change thermal storage systems. Renew Sustain Energy Rev 2012;16(4):2118–32.
[11] Zalba B, Marıń JM, Cabeza LF, Mehling H. Review on thermal energy storage with phase change: materials, heat transfer analysis and applications. Appl Therm Eng 2003;23(3):251–83.
[12] Harikrishnan S, Deenadhayalan M, Kalaiselvam S. Experimental investigation of solidification and melting characteristics of composite PCM(s) for building heating application. Energy Convers Manage 2014;86:864–72.
[13] Amin NAM, Bruno F, Belusko M. Effectiveness-NTU correlation for low temperature PCM encapsulated in spheres. Appl Energy 2012;93:549–55.
[14] Amin NAM, Bruno F, Belusko M. Effective thermal conductivity for melting in PCM encapsulated in a sphere. Appl Energy 2014;122:280–7.
[15] Gil A, Medrano M, Martorell I, Lazaro A, Dolado P. Zalba B, Cabeza LF. State of the art on high temperature thermal energy storage for power generation. Part 1—concepts, materials and modellization. Renew Sustain Energy Rev 2010;14(1):31–55.
[16] Jacob R, Belusko M, Fernández AI, Cabeza LF, Saman W, Bruno F. Embodied energy and cost of high temperature thermal energy storage systems for use with concentrated solar power plants. Appl Energy 2016;180:586–97.
[17] Liu M, Tay NS, Bell S, Belusko M, Jacob R, Will G, et al. Review on concentrating solar power plants and new developments in high temperature thermal energy storage technologies. Renew Sustain Energy Rev 2016;53:1411–32.
[18] Galione P, Pérez-Segarra CD, Rodríguez I, Torras S, Rigola J. Multi-layered solid-PCM thermocline thermal storage for CSP. Numerical evaluation of its application in a 50 MWe plant. Sol Energy 2015;119:134–50.
[19] Galione P, Pérez-Segarra CD, Rodríguez I, Oliva A, Rigola J. Multi-layered solid-PCM thermocline thermal storage concept for CSP plants. Num Anal Persp Appl Energy 2015;142:337–51.
[20] Zhao BC, Cheng MS, Liu C, Min-Dai Z. Thermal performance and cost Analysis of a multi-layered solid-PCM thermocline thermal energy storage for CSP tower plants. Appl Energy 2016;178:784–99.
[21] Zanganeh G, Medrano M, Commerford M, Haselbacher A, Pedretti A, Steinfeld A. Stabilization of the outflow temperature of a packed-bed thermal energy storage by combining rocks with phase change materials. Appl Therm Eng 2014;70:316–20.
[22] Flueckiger SM, Garimella SV. Latent heat augmentation of thermocline energy storage for concentrating solar power -a system-level assessment. Appl Energy 2014;116:278–87.
[23] Cheng X, Zhai X, Wang R. Thermal performance analysis and optimization of a cascaded packed bed cool thermal energy storage unit using multiple phase change materials. Appl Energy 2018;215:566–76.
[24] Wu M, Xu C, He YL. Dynamic thermal performance analysis of a molten-salt packed-bed thermal energy storage system using PCM capsules. Appl Energy 2014;121:184–95.
[25] Yang L, Zhang X, Xu G. Thermal performance of a solar storage packed bed using spherical capsules filled with PCM having different melting points. Energy Build 2014;68(Part B):639–46.
[26] Rady M. Thermal performance of packed bed thermal energy storage units using multiple granular phase change composites. Appl Energy 2009;86:2704–20.
[27] Tehrani SSM, Shoraka Y, Nithyanandam K, Taylor RA. Cyclic performance of cascaded and multi-layered solid-PCM shell-and-tube thermal energy storage systems: a case study of the 19.9 MWe Gemasolar CSP plant. Appl Energy 2018;288:240–53.
[28] Aldoss TK, Rahman MM. Comparison between the single-PCM and multi-PCM thermal energy storage design. Energy Convers Manage 2014;83:79–87.
[29] Li D, Hu Y, Li D, Wang J. Combined-cycle gas turbine power plant integration with cascaded latent heat thermal storage for fast dynamic responses. Energy Convers Manage 2019;183:1–13.
[30] Peng Q, Yang X, Ding J, Wei X, Yang J. Design of new molten salt thermal energy storage material for solar thermal power plant. Appl Energy 2013;112:682–9.
[31] Vignarooban K, Xu X, Arvay A, Hsu K, Kannan AM. Heat transfer fluids for concentrating solar power systems - a review. Appl Energy 2015;146:383–96.
[32] Nithyanandam K, Pitchumani R, Mathur A. Analysis of a latent thermocline storage system with encapsulated phase change materials for concentrating solar power. Appl Energy 2014;113:1446–60.
[33] Ismail KAR, Henriquez JR. Numerical and experimental study of spherical capsules packed bed latent heat storage system. Appl Therm Eng 2002;22:1705–16.
[34] Yang Z, Garimella SV. Cyclic operation of molten-salt thermal energy storage in thermoclines for solar power plants. Appl Energy 2013;103:256–65.
[35] Esence T, Bruch A, Molina S, Stutz B, Fourmigue JF. A review on experience feedback and numerical modeling of packed bed thermal energy storage systems. Sol Energy 2017;153:628–54.
[36] Xu C, Li X, Wang Z, He Y, Bai F. Effects of solid particle properties on the thermal performance of a packed-bed molten-salt thermocline thermal storage system. Appl Therm Eng 2013;57:69–80.
[37] Liu M, Gomez JC, Turchi CS, Tay NHS, Saman W, Bruno F. Determination of

thermo-physical properties and stability testing of high-temperature phase-change materials for CSP Applications. Sol Energy Mater Sol Cells 2015;139:81–7.
[38] Wakao N, Kaguei S. Heat and mass transfer in packed beds. New York: Gordon and Breach Science Publishers; 1982.
[39] VDI-Gesellschaft, VDI-Wärmeatlas, 10th ed. Berlin: Springer; 2006.
[40] Wakao N, Kaguei S, Funazkri T. Effect of fluid dispersion coefficients on particle to fluid heat transfer coefficients in packed beds: correlation of Nusselt numbers. Chem Eng Sci 1979;34:325–36.
[41] Incropera FP, DeWitt DP, Bergman TL, Lavine AS. Fundamentals of heat and mass transfer. 6th ed. USA: SOS Free Stock; 2007.
[42] Peng H, Dong H, Ling X. Thermal investigation of PCM-based high temperature thermal energy storage in packed bed. Energy Convers Manage 2014;81:420–7.
[43] Gunarathne DS, Chmielewski JK, Weihong Y. Pressure drop prediction of a gasifier bed with cylindrical biomass pellets. Appl Energy 2014;113:258–66.
[44] Bindra H, Bueno P, Morris JF, Shinnar R. Thermal analysis and exergy evaluation of packed bed thermal storage systems. Appl Therm Eng 2013;52:255–63.
[45] Jegadheeswaran S, Pohekar SD, Kousksou T. Exergy based performance evaluation of latent heat thermal storage system: a review. Renew Sustain Energy Rev 2010;14:2580–95.
[46] Hänchen M, Brückner S, Steinfeld A. High-temperature thermal storage using a packed bed of rocks – heat transfer analysis and experimental validation. Appl Therm Eng 2011;31:1798–806.
[47] Pacheco JE, Showalter SK, Kolb WJ. Development of a molten-salt thermocline thermal storage system for parabolic trough plants. J Sol Energy Eng 2002;124:153–9.